RSC Advances

PAPER

View Article Online
View Journal | View Issue

Cite this: *RSC Adv.*, 2017, **7**, 2242

A sensitive non-enzymatic immunosensor composed of silver nanoflowers for squamous cell carcinoma antigen†

Yueyun Li,[ab] Yihe Zhang,*[a] Jian Han,[b] Paul K. Chu,[c] Jinhui Feng[b] and Yunhui Dong[b]

Received 7th November 2016
Accepted 30th November 2016

DOI: 10.1039/c6ra26438g

www.rsc.org/advances

In this work, a sensitive sandwich-type non-enzymatic electrochemical immunosensor for quantitative detection of squamous cell carcinoma antigen (SCCA) is designed and fabricated. Gold nanoparticles/graphene nanoribbons (Au NPs/NH_2–GNRs) are used as the platform of electrochemical immunosensor to accelerate electron transfer and increase the specific surface area. The Au NPs with good biocompatibility can increase the probability of capturing primary antibodies (Ab_1) to further improve the sensitivity. The silver nanoflower–molybdenum disulfide/multiwalled carbon nanotubes (SNFs–NH_2–MoS_2/MWCNTs) were used as labels of secondary antibodies (Ab_2) and exhibit remarkable multiple-signal amplification effects. The silver nanoflowers with many branches can provide abundant active sites for the electrochemical reaction to further improve the sensitivity. Under the optimal conditions, the immunosensor shows a wide linear range between 0.1 pg mL^{-1} and 20 ng mL^{-1} with a limit of detection 0.03 pg mL^{-1}. Furthermore, the novel immunosensor shows good performance for the detection of serum samples. The results indicate that the proposed immunosensor could be promising in the clinical application for quantitative detection of SCCA.

1. Introduction

Squamous cell carcinoma antigen (SCCA), a member of the high molecular weight family of seine protease inhibitors (serpins), is related to a number of different epithelial cancers.[1,2] The SCCA levels coincide with tumor infiltration and the frequency of lymph node metastasis in both esophageal squamous cell carcinomas and cervical.[3–6] Hence, it is necessary to develop a simple, rapid, and accurate quantitative method for SCCA. Among the various analytical techniques, the electrochemical immunosensor has made rapid progress due to advantages such as the short analysis time, fast response, simple operation, simple instrumentation, low cost, reliability, high sensitivity, and good selectivity.[7] In this work, a novel electrochemical immunosensor is designed and fabricated for quantitative monitoring of SCCA.

In this work, some new materials were proposed in order to achieve quantitative detection of SCCA and improve the sensitivity of the immunosensor. Graphene nanoribbons (GNRs) have attracted much attention in nanodevices[8,9] and are used as support for dispersion of nanoparticles due to desirable properties such as high electrical conductivity, large surface area, and electrochemical stability in acidic and alkaline electrolytes.[9] Gold nanoparticles (Au NPs) can be easily and firmly fixed on GNRs when amino groups are introduced to the surface of GNRs. Au NPs are usually used in non-enzymatic immunosensors because of the good electrical conductivity, biocompatibility, as well as nontoxicity.[10–12] Thus, in this work, the composite materials have been used to immobilize antibodies on electrodes, improve the electrical conductivity and improve the sensitivity of the immunosensor.

The labels of secondary anti-bodies were also well-designed to further improve the sensitivity of the immunosensor. Molybdenum disulfide (MoS_2), a two-dimensional (2D) layered transition metal dichalcogenide (LTMDs), has attracted increasing interest due to the unique structure and properties and potential application to energy storage, catalysis, optoelectronics, and electronics.[13–16] The free energy of atomic hydrogen bonding to the sulfur edge of the MoS_2 structure is close to that of Pt indicting MoS_2 a potential substitutes for Pt-group catalysts.[17,18] In fact, MoS_2 as a supporter and label of the secondary antibodies can improve the sensitivity of immunosensors. However, MoS_2 nanosheets have the tendency to restack due to the high surface energy and van der Waals force. In order to overcome these hurdles, MWCNTs, as one member of the family of carbon family with good electrical, chemical,

[a]*Beijing Key Laboratory of Materials Utilization of Nonmetallic Minerals and Solid Wastes, National Laboratory of Mineral Materials, School of Materials Science and Technology, China University of Geosciences, Beijing, 100083, P. R. China. E-mail: zyhcugb@163.com; Fax: +86-010-82323433; Tel: +86-010-82323433*

[b]*School of Chemical Engineering, Shandong University of Technology, Zibo, 255049, P. R. China*

[c]*Department of Physics & Materials Science, City University of Hong Kong, Tat Chee Avenue, Kowloon, Hong Kong, China*

† Electronic supplementary information (ESI) available. See DOI: 10.1039/c6ra26438g

and mechanical properties,[19–21] have been incorporated into MoS_2 sheets to minimize or prevent aggregation of the MoS_2 sheets[13] and also improve the electroconductivity of the combination. Silver nanoflowers (SNFs), an environmentally friendly and non-toxic catalyst with high activity, can easily connect with the amino group on the surface of MoS_2/MWCNTs. The MoS_2/MWCNTs hybrid also obtained excellent electrochemical properties due to the synergistic effects between MWCNTs and MoS_2.[22] MoS_2/MWCNTs as the support for the growth of SNFs can control the suitable size of SNFs. The larger size of SNFs than silver nanoparticles can reduce the possibility that SNFs were fasten onto the surface of immunosensor through physical adsorption. The abundant branches of SNFs can provide a lot of active site for the electrochemical reaction. Simultaneously, the good catalytic performance in H_2O_2 reduction can further improve the sensitivity of immunosensors.[23–25]

In this work, a novel electrochemical immunosensor is successfully fabricated and applied for the quantitative analysis of SCCA. The Au NPs/NH_2–GNRs as the platform of electrochemical immunosensor can improve the electroconductivity and provide a large specific surface area to increase the loading of antibodies. The SNFs–NH_2–MoS_2/MWCNTs as the labels of secondary antibodies can not only provide a large specific surface area for the immobilization of secondary antibodies, but also provide good electro-catalytic activity for the reduction of H_2O_2 to improve the sensitivity, accuracy, and detection limit.

2. Experimental details

2.1. Regents and apparatus

The SCCA antibodies were purchased from Beijing Dingguo Changsheng Biotechnology Co. Ltd. (China), bovine serum albumin (BSA) from Sigma-Aldrich (Beijing, China), multi-walled carbon nanotubes (MWCNTs) from Alfa Aesar Co., Ltd. (Shanghai, China), and $HAuCl_4 \cdot 4H_2O$ from Sigma-Aldrich Co., Ltd. (Beijing, China). The phosphate buffered solution (PBS, 1/15 mol L^{-1} KH_2PO_4 and 1/15 mol L^{-1} Na_2HPO_4) was used as the electrolyte in the electrochemical assessment. All the other chemical reagents were analytical reagent grade and used without purification.

Cyclic voltammetry (CV), amperometry (*i–t* curves), and electrochemical impedance spectroscopy (EIS) were conducted on the CHI 760D electrochemical workstation (Shanghai Chenhua Instrument Co. Ltd., China) using a conventional three-electrode system with the a modified glassy carbon electrode (GCE, $\Phi = 4$ mm) being the working electrode, platinum wire electrode being the counter electrode, and saturated calomel electrode (SCE) being the reference electrode. The morphology of GNRs, Au NPs/NH_2–GNRs, NH_2–MoS_2/MWCNT, and SNFs–NH_2–MoS_2/MWCNT was examined by scanning electron microscopy (SEM, JSM-6700F microscope, JEOL, Japan) and the X-ray diffraction (XRD) patterns were obtained on the Rigaku D/max 2550 VB + 18 kW X-ray diffractometer with Cu K_α radiation (0.1542 nm).

2.2. Measurement methods

In this work, H_2O_2 was used as the redox probe to monitor electron transfer from H_2O_2 to the electrode in the electrochemical reaction. In the amperometric *i–t* curves, −0.5 V was selected as the detection potential. The current change was recorded when 5 mol L^{-1} H_2O_2 (10 μL) was added to the buffer solution (10 mL) and the analysis result was established based on the currents for various SCCA concentrations.

2.3. Preparation of Au NPs/NH_2–GNRs

Preparation of graphene oxide nanoribbons (GONRs). The preparation procedures of the GONRs are similar to those reported in the literatures.[26,27] In brief, the MWCNTs (30 mg) were suspended in H_2SO_4 (30 mL) for 12 h and $KMnO_4$ (150 mg) was added to the mixture. The suspension was stirred continuously for 1 h at 20 °C and heated to 55 °C in a water bath for 30 min and then 65 °C for 4 h. The reaction was completed when the mixture became yellow/brown and the temperature was increased to 70 °C for another 10 minutes. The suspension was removed from the water bath, cooled to room temperature, and poured into 400 mL of ice containing 5 mL of H_2O_2 (30%). The sediment was obtained after centrifugation and cleaning with deionized water and ether. The final product of GONRs was obtained after dried at 60 °C.

Preparation of NH_2–GNRs. The NH_2–GNRs were prepared according to a previous method.[28] In the typical experiment, 100 mg of GONRs were added to 40 mL of ethylene glycol under ultrasonication. Then 1 mL of ammonium hydroxide (6 mol L^{-1}) was added and the color changed to dark brown. Subsequently, the dark brown solution was sealed in a Teflon-lined stainless steel autoclave for solvothermal reaction at 180 °C for 10 h. After reaction, the mixture was centrifuged and washed three times with deionized water and ethanol. The NH_2–GNRs were obtained after drying at 65 °C for 24 h.

Synthesis of Au NPs/NH_2–GNRs. Preparation of Au NPs was in accordance with the procedures described in the literature with minor changes.[29] 100 mL of the solution containing 4.12 mL of $HAuCl_4$ (1 wt%) and 95.88 mL of deionized water were refluxed at 100 °C. 10 mL of sodium citrate (38.8 mmol L^{-1}) were added under magnetic stirring and refluxed for 15 min. The solution was cooled to room temperature and centrifuged. A wine red solution with the Au NPs was obtained and 10 mg of NH_2–GNRs were added. The Au NPs/NH_2–GNRs were obtained after centrifugation and drying.

Dispersion of Au NPs/NH_2–GNRs. 500 μL of glacial acetic acid were diluted with 100 mL of ultrapure water and 50 mg of chitosan were added. Various concentrations of Au NPs/NH_2–GNRs were prepared in the solution.

2.4. Preparation of SNFs–NH_2–MoS_2/MWCNT

Synthesis of MoS_2/MWCNT. Preparation of MoS_2/MWCNTs was in accordance with previous literature with minor changes.[30] 38.5 mg of S powders, 92.7 mg of ammonium molybdate $[(NH)_6Mo_7O_{24} \cdot 4H_2O]$, and 100 mg MWCNTs were added to a solution of ethanol (13 mL) and octylamine (14 mL).

The suspension was obtained after stirred for 20 min and transferred to a Teflon stainless steel autoclave, sealed, and heated at 200 °C for 24 h in an oven. After cooling to room temperature naturally, the precipitate was collected by centrifugation, rinsed several times with ethanol and ultrapure water, and dried in vacuum at 60 °C for 10 h to obtain the precursor MoS_2/MWCNTs.

Synthesis of SNFs–NH_2–MoS_2/MWCNT. The synthesis method for the NH_2–MoS_2/MWCNT was similar to that for the NH_2–GNRs. In the typical synthesis,[31] 100 mL of an aqueous solution of $AgNO_3$ (1 mmol mL^{-1}) and 10 mg of NH_2–MoS_2/MWCNT were stirred for 30 min and 2 mL of rutin (15 mmol mL^{-1}) were added. The suspension was stirred continuously for 30 min and then the sediment was obtained after centrifugation and drying.

2.5. Preparation of Ab_2–SNFs–NH_2–MoS_2/MWCNT

The SNFs–NH_2–MoS_2/MWCNTs were dispersed in PBS (pH = 7.4) together with excess SCCA antibodies (100 μg mL^{-1}). The mixture was incubated in a shaker/incubator for 12 h at 4 °C, centrifuged, and washed to remove unbound antibodies. The sediment was again dispersed in PBS and stored at 4 °C when not used.

2.6. Fabrication of the immunosensor

The GCE was polished to a mirror surface with alumina slurry, sonicated in ethanol for 30 s, and rinsed with ultrapure water. The GCE was covered with 6.0 μL of the Au NPs/NH_2–GNRs solution and dried in air. 6.0 μL of the Ab_1 solution were dropped onto the surface of the electrode and after drying in air, 6.0 μL of the BSA (0.1%) solution covered the electrode in order to block nonspecific binding between the SCCA and substrate. The immunosensor was thoroughly washed with PBS (pH = 7.4) and dried. 6.0 μL of SCCA solutions with different concentrations were dropped onto the electrode for 1 h at room temperature to ensure specific binding between the antibodies and antigen. Finally, 6.0 μL of the Ab_2–SNFs–NH_2–MoS_2/MWCNT solution were modified onto the electrode and dried at room temperature. The immunosensor was washed with PBS to remove unbound labels-Ab_2. Fig. 1 illustrates the fabrication procedures for the immunosensor.

3. Results and discussion

3.1. Characterization

Fig. 2A and B show the SEM micrographs of the GNRs and Au NPs/NH_2–GNRs. The Au NPs are distributed uniformly on the GNRs and the Au NPs/NH_2–GNRs are fabricated. Fig. 2C shows the SEM images of the flower-like silver structures. The length of the SNFs is about 2 μm and the diameter of the branch is about 100 nm. The morphology of the layered MoS_2 is examined by SEM (Fig. 2D). The MoS_2 nanosheets are uniform with an average diameter of about 200 nm. The SEM image of the MoS_2/MWCNTs (Fig. 2E) shows that the MWCNTs are inserted into the lamellar structure of MoS_2. Fig. 2F depicts the SEM image of the SNFs–NH_2–MoS_2/MWCNTs. The SNFs are distributed uniformly on the surface of MoS_2/MWCNTs and shorten due to MoS_2/MWCNTs being the support. Fig. 2G shows the XRD patterns of the MWCNTs, MoS_2, MoS_2/MWCNTs and SNFs–NH_2–MoS_2/MWCNTs composite. The peaks at 26.4°, 42.2°, 44.4°, 54.5°, and 77.2° in the diffraction pattern of MWCNTs are attributed to the hexagonal graphite structures (002), (100), (101), (004), and (110) (curve a). The diffraction peaks at 16.3°, 32.6°, and 56.7° correspond to the (002), (100), and (110) diffraction planes of MoS_2 (curve b) and those at 38.1°, 44.3°, 64.4°, and 77.5° arise from the (111), (200), (220), and (311) crystalline planes of Ag (curve d). Fig. 2H shows the presence of C, Mo, S and Ag element result indicates that the attached NPs on MoS_2/MWCNTSs are SNFs.

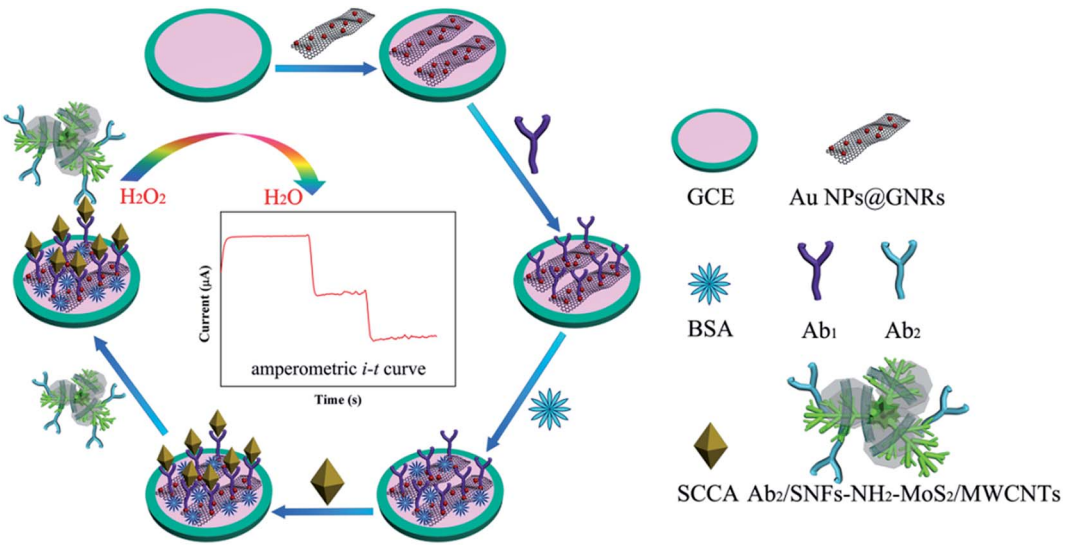

Fig. 1 Fabrication of the immunosensor.

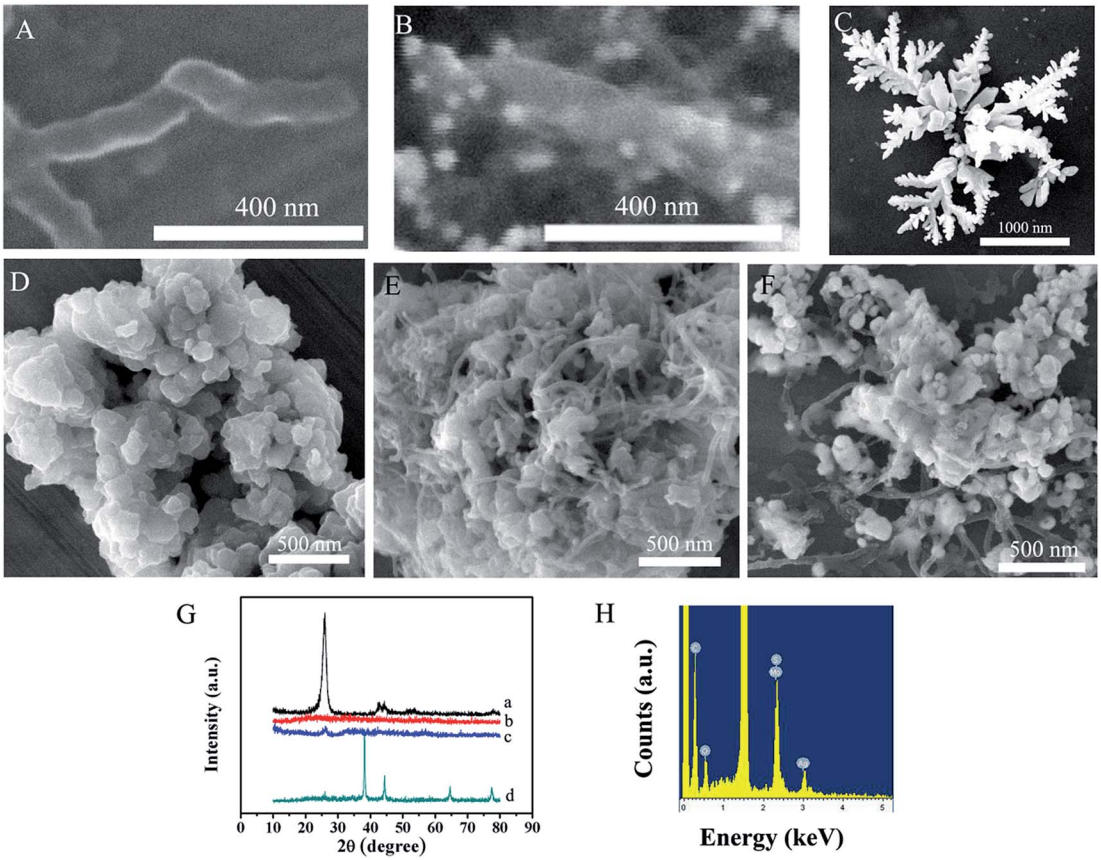

Fig. 2 SEM images: (A) GNRs, (B) Au NPs/NH_2–GNRs, (C) SNFs, (D) MoS_2, (E) MoS_2/MWCNTSs, and (F) SNFs–NH_2–MoS_2/MWCNTSs; (G) XRD of (a) MWCNTs (b) MoS_2, (c) MoS_2/MWCNTSs, and (d) SNFs–NH_2–MoS_2/MWCNTSs; (H) EDS of SNFs–NH_2–MoS_2/MWCNTSs.

3.2. Characterization of the immunosensor

Each immobilization steps is monitored by EIS which is a well-established technique to monitor the features of surface-modified electrodes.[32,33] The Nyquist diagrams show two parts: a semicircle at high frequencies and linear region at low frequencies. The semicircle at high frequencies shows that the electron transfer resistance (R_{et}) corresponds to the electron-transfer-limited process and the linear portion at low frequencies correspond to diffusion.[34,35] As shown in Fig. 3, EIS is performed for each modification stage of immunosensor in the $[Fe(CN)_6]^{3-/4-}$ (5 mmol L^{-1}) solution containing KCl (0.1 mol L^{-1}). A well-defined semicircle of GCE is observed at high frequencies (curve a). A smaller semicircle is observed when Au NPs/NH_2–GNRs were covered the electrode, indicating that the Au NPs/NH_2–GNRs can accelerate electron transfer (curve b). However, the semicircle diameter successively increased when Ab_1 (curve c), BSA (curve d), SCCA (curve e), labels-Ab_2 (curve f) were covered on the electrode respectively, illustrating that the subsequent modification (Ab_1, BSA, SCCA, labels-Ab_2) hinder electron transfer to the electrode. These modifications belongs to protein which is disadvantaged for the electronic transmission, thus, each additional layer was dropped onto the surface of electrode can increase the resistance. The result can also demonstrate that the immunosensor were fabricated successfully.

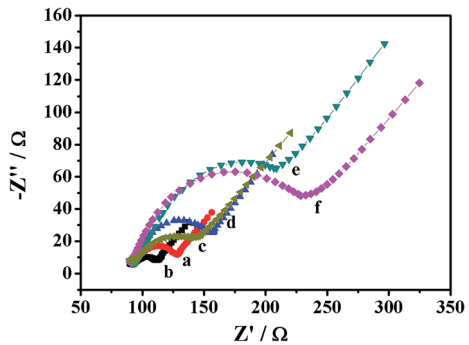

Fig. 3 EIS of (a) GCE, (b) GCE/Au NPs/NH_2–GNRs, (c) GCE/Au NPs/NH_2–GNRs/Ab_1, (d) GCE/Au NPs/NH_2–GNRs/Ab_1/BSA, (e) GCE/Au NPs/NH_2–GNRs/Ab_1/BSA/SCCA, and (f) GCE/Au NPs/NH_2–GNRs/Ab_1/BSA/Ab_2–SNFs–NH_2–MoS_2/MWCNTSs.

3.3. Optimization of conditions

To compare the catalytic performance of various kinds of materials in H_2O_2 reduction, the amperometric *i–t* curves are presented in Fig. 4A. The Au NPs/NH_2–GNRs only have mild catalytic ability towards H_2O_2 reduction (curve a). Good catalytic performance is shown MoS_2/MWCNTs are placed on the electrode (curve b) and a large current change is detected when

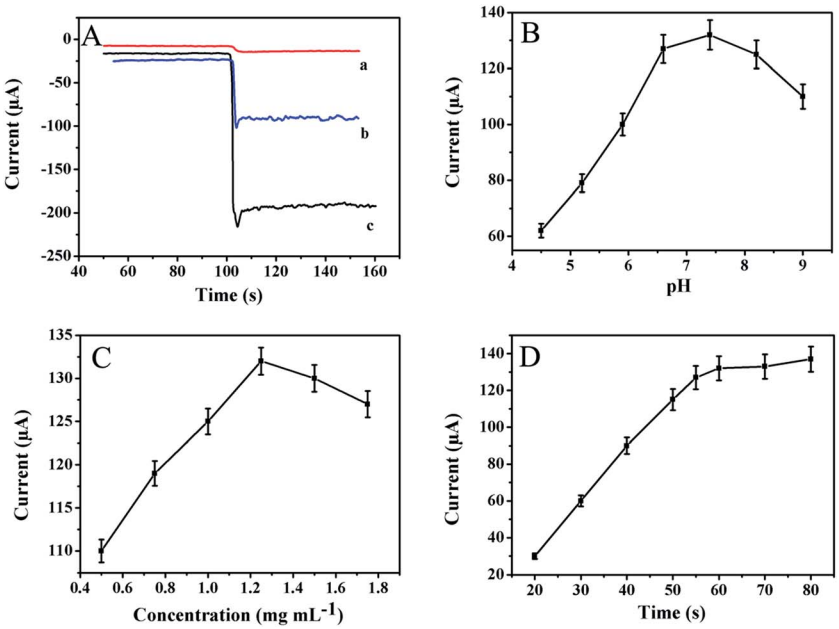

Fig. 4 (A) Amperometric response of the immunosensor with different labels: (a) Au NPs/NH_2–GNRs, (b) MoS_2/MWCNT, and (c) SNFs–NH_2–MoS_2/MWCNT; optimization of experimental conditions: (B) pH, (C) Au NPs/NH_2–GNRs concentration, and (D) incubation time.

SNFs–NH_2–MoS_2/MWCNTs cover the electrode (curve c). The results show that SNFs–NH_2–MoS_2/MWCNTs are good catalytic materials for H_2O_2 and SNFs–NH_2–MoS_2/MWCNTs as a label for secondary antibodies can produce satisfactory sensitivity.

It is important to optimize the experimental conditions for the accuracy and sensitivity of immunosensor. Here, the pH value of the electrolyte, concentration of Au NPs/NH_2–GNRs, and incubation time are in the quantitative determination of SCCA. As shown in Fig. 4B, the amperometric response increases with pH value until 7.4 and then decreases with the increase of pH value. Thus, the optimal pH is 7.4. Because either acidic or alkaline conditions may damage proteins.[36] As shown in Fig. 4C, the concentration of Au NPs/NH_2–GNRs is another important parameter. At first, the amperometric response increases with the concentration of Au NPs/NH_2–GNRs but when the concentration reaches 1.25 mg mL^{-1} the response with a slow growth. The result revealed that a moderate amount of Au NPs/NH_2–GNRs provides a large contacting area and increases the electron conductivity. However, the electron conductivity of Au NPs/NH_2–GNRs cannot offset the layer resistance at high concentrations. The optimal concentration is 1.25 mg mL^{-1}. Fig. 4D shows the influence of incubation time. The response increases sharply before 60 min but slows afterwards. Therefore, the optimal time is 60 min. To summarize, the optimal pH value is 7.4, concentration of Au NPs/NH_2–GNRs is 1.25 mg mL^{-1}, and incubation time is 60 min.

3.4. Analytical performance

The amperometric response of the immunosensor is studied in the detection of SCCA by the amperometric *i*–*t* curve under the optimal conditions. As shown in Fig. 5A, the plot is $I = 26.27 \lg c$ (c, ng mL^{-1}) + 105.4, $R = 0.988$. The immunosensor exhibits a wide linear range from 0.1 pg mL^{-1} to 20 ng mL^{-1} with

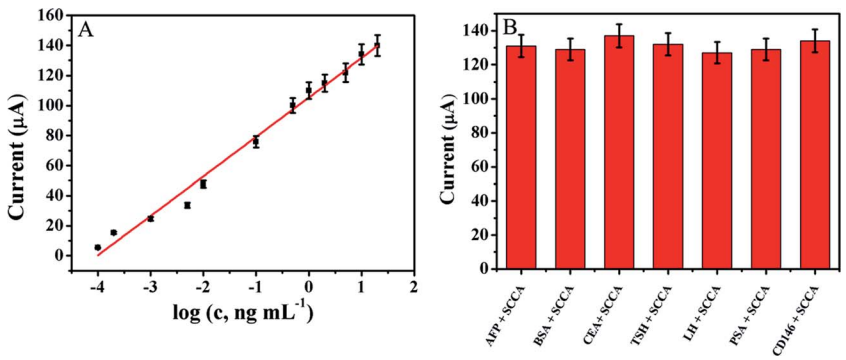

Fig. 5 Calibration curve of the immunosensor for different concentrations of SCCA: (A) sandwich-type immunosensor, (B) currents in the presence of interfering substances (500 ng mL^{-1}) and SCCA (10 ng mL^{-1}). (Error bar = SE, $n = 5$).

a detection limit of 0.03 pg mL^{-1}. The immunosensor has good sensitivity and a low detection limit which were ascribed to three reasons: (1) the Au NPs/NH_2–GNRs have good electron conductivity and Au NPs can immobilize the antibodies; (2) the MWCNTs increase the specific surface area and prevent or minimize aggregation the MoS_2. (3) The synergistic catalytic effects of MoS_2 and SNFs for H_2O_2 improve the sensitivity of the immunosensor. A series of studies is performed for quantitative detection of SCCA and the electrochemical immunosensor based on SNFs–NH_2–MoS_2/MWCNT indeed shows a wide linear range and low detection limit (Table S1 in ESI†) boding well for clinical application.

3.5. Reproducibility, stability, and selectivity

To investigate the reproducibility of the immunosensor, five electrodes are prepared for the detection of 10 ng mL^{-1} of SCCA under the same conditions. The relative standard deviation (RSD) is 4.7%, which indicates that the reproducibility of designed immunosensor is excellent. To investigate the selectivity, different interfering substances including alpha fetal protein (AFP), bovine serum albumin (BSA), carcino embryonic antigen (CEA), thyroid stimulating hormone (TSH), luteinizing hormone (LH), prostate protein antigen (PSA), and melanoma adhesion molecule antigen (CD146) are used. The SCCA (10 ng mL^{-1}) solution containing 500 ng mL^{-1} of the interfering substances is measured by the immunosensor and the results are presented in Fig. 5B. The change of current is less than 5% compared to that without interferences confirming the good selectivity.

3.6. Real samples

To evaluate the accuracy and precision of the immunosensor for real samples, various concentrations of SCCA were detected by the standard addition method (Table S2 in ESI†). Samples with different concentrations of 0.50, 1.00, and 5.00 ng mL^{-1} are added to the serum samples, respectively. The RSD is less than 7% and the recovery rate ranges from 96% to 100.04%, indicating that the proposed immunosensor could be effectively applied to the clinical determination of the SCCA levels in human serum samples.

4. Conclusion

In summary, a novel electrochemical immunosensor is designed and fabricated for quantitative detection of SCCA. The Au NPs/NH_2–GNRs are used as the substrate to expedite electron transfer and improve the sensitivity due to the large specific surface area captured more antibodies. The SNFs–NH_2–MoS_2/MWCNTs are used as the labels of secondary antibodies can further improve the sensitivity due to their good catalytic performance in H_2O_2 reduction. The immunosensor exhibits a broad linear range, low detection limit, as well as good reproducibility, sensitivity, and selectivity and have promising applications in clinical diagnosis.

Acknowledgements

This study was jointly supported by the National Natural Science Foundation of China (No. 21575079; 21575050; 51572246); National High Technology Research and Development Program (863 Program 2012AA06A109) of China, Project of Shandong Province Higher Educational Science and Technology Program (No. J14LC09), Hong Kong Research Grant Council (RGC) General Research Funds (GRF) No. CityU 11301215.

References

1 G. Giannelli, F. Marinosci, C. Sgarra, L. Lupo, P. Dentico and S. Antonaci, *Int. J. Cancer*, 2005, **116**, 579–583.
2 H. Kato and T. Torigoe, *Cancer*, 1977, **40**, 1621–1628.
3 J. M. Duk, H. W. de Bruijn, K. H. Groenier, H. Hollema, A. Klaske, M. Krans and J. G. Aalders, *Gynecol. Oncol.*, 1990, **39**, 186–194.
4 J. M. Catanzaro, J. L. Guerriero, J. Liu, E. Ullman, N. Sheshadri, J. J. Chen and W. X. Zong, *PLoS One*, 2011, **6**, e19096.
5 H. Shimada, Y. Nabeya, S.-i. Okazumi, H. Matsubara, T. Shiratori, Y. Gunji, S. Kobayashi, H. Hayashi and T. Ochiai, *Surgery*, 2003, **133**, 486–494.
6 N. Takeshima, Y. Hirai, K. Katase, K. Yano, K. Yamauchi and K. Hasumi, *Gynecol. Oncol.*, 1998, **68**, 263–266.
7 K. R. Rogers, J. Y. Becker, J. Wang and F. Lu, *Field Anal. Chem. Technol.*, 1999, **3**, 161–169.
8 M. Y. Han, B. Özyilmaz, Y. Zhang and P. Kim, *Phys. Rev. Lett.*, 2007, **98**, 206805.
9 Z. Chen, Y.-M. Lin, M. J. Rooks and P. Avouris, *Phys. E*, 2007, **40**, 228–232.
10 S. Mehmood, A. Naeem, S. Sabahat, R. Ciancio, E. Carlino, M. F. Bhopal and A. S. Bhatti, *Superlattices Microstruct.*, 2015, **81**, 248–264.
11 Y. Zhuo, R. Yuan, Y. Chai, D. Tang, Y. Zhang, N. Wang, X. Li and Q. Zhu, *Electrochem. Commun.*, 2005, **7**, 355–360.
12 V. Mani, B. V. Chikkaveeraiah, V. Patel, J. S. Gutkind and J. F. Rusling, *ACS Nano*, 2009, **3**, 585–594.
13 S. Zhang, B. Chowdari, Z. Wen, J. Jin and J. Yang, *ACS Nano*, 2015, **9**, 12464–12472.
14 M. Yang, J. Zhang and X. Chen, *J. Electroanal. Chem.*, 2015, **736**, 88–92.
15 L. Yu, Y.-H. Lee, X. Ling, E. J. Santos, Y. C. Shin, Y. Lin, M. Dubey, E. Kaxiras, J. Kong and H. Wang, *Nano Lett.*, 2014, **14**, 3055–3063.
16 M. S. Choi, D. Qu, D. Lee, X. Liu, K. Watanabe, T. Taniguchi and W. J. Yoo, *ACS Nano*, 2014, **8**, 9332–9340.
17 X. Ren, Q. Ma, H. Fan, L. Pang, Y. Zhang, Y. Yao, X. Ren and S. F. Liu, *Chem. Commun.*, 2015, **51**, 15997–16000.
18 T. Wang, L. Liu, Z. Zhu, P. Papakonstantinou, J. Hu, H. Liu and M. Li, *Energy Environ. Sci.*, 2013, **6**, 625–633.
19 F. Valentini, S. Orlanducci, M. L. Terranova, A. Amine and G. Palleschi, *Sens. Actuators, B*, 2004, **100**, 117–125.
20 M. Trojanowicz, *TrAC, Trends Anal. Chem.*, 2006, **25**, 480–489.

21 M. a. D. Rubianes and G. A. Rivas, *Electrochem. Commun.*, 2003, **5**, 689–694.
22 M. Zheng, J. Huo, Y. Tu, J. Wu, L. Hu and S. Dai, *Electrochim. Acta*, 2015, **173**, 252–259.
23 Z. Sun, G. Cui, H. Li, Y. Tian and S. Yan, *Colloids Surf., A*, 2016, **489**, 142–153.
24 T. Ji, L. Chen, M. Schmitz, F. S. Bao and J. Zhu, *Green Chem.*, 2015, **17**, 2515–2523.
25 Y. He, G. Huang, Z. Pan, Y. Liu, Q. Gong, C. Yao and J. Gao, *Mater. Res. Bull.*, 2015, **70**, 263–271.
26 D. V. Kosynkin, A. L. Higginbotham, A. Sinitskii, J. R. Lomeda, A. Dimiev, B. K. Price and J. M. Tour, *Nature*, 2009, **458**, 872–876.
27 Y. X. Huang, X. W. Liu, J. F. Xie, G. P. Sheng, G. Y. Wang, Y. Y. Zhang, A. W. Xu and H. Q. Yu, *Chem. Commun.*, 2011, **47**, 5795–5797.
28 L. Lai, L. Chen, D. Zhan, L. Sun, J. Liu, S. H. Lim, C. K. Poh, Z. Shen and J. Lin, *Carbon*, 2011, **49**, 3250–3257.
29 G. Frens, *Nature*, 1972, 20–22.
30 L. Ren, G. Zhang, Z. Yan, L. Kang, H. Xu, F. Shi, Z. Lei and Z. H. Liu, *ACS Appl. Mater. Interfaces*, 2015, **7**, 28294–28302.
31 T. Liu, D. Li, D. Yang and M. Jiang, *Langmuir*, 2011, **27**, 6211–6217.
32 J. R. Macdonald, *J. Electroanal. Chem. Interfacial Electrochem.*, 1987, **223**, 25–50.
33 K. Eckhard, H. Shin, B. Mizaikoff, W. Schuhmann and C. Kranz, *Electrochem. Commun.*, 2007, **9**, 1311–1315.
34 R. Cui, H. Huang, Z. Yin, D. Gao and J.-J. Zhu, *Biosens. Bioelectron.*, 2008, **23**, 1666–1673.
35 F. J. Santaclara, R. I. Pérez-Martín and C. G. Sotelo, *Food Chem.*, 2014, **143**, 22–26.
36 Y. Cai, H. Li, B. Du, M. Yang, Y. Li, D. Wu, Y. Zhao, Y. Dai and Q. Wei, *Biomaterials*, 2011, **32**, 2117–2123.